A Cryogenic Current Comparator for the Low Energy Antiproton Facilities at CERN

M. Fernandes; J. Tan

CERN – Geneva/CH

C.P. Welsch

Cockcroft Institute & The University of Liverpool, Liverpool/UK

Abstract

Several laboratories have shown the potential of using Superconducting Quantum Interference Device (SQUID) magnetometers together with superconductor magnetic shields to measure beam current intensities in the submicro-Ampere regime. CERN, in collaboration with GSI, Jena University and Helmholtz Institute Jena, is currently working on developing an improved version of such a current monitor for the Antiproton Decelerator (AD) and Extra Low ENergy Antiproton (ELENA) rings at CERN, aiming for better current resolution and overall system availability. This contribution will present the current design, including theoretical estimation of the current resolution; stability limits of SQUID systems and adaptation of the coupling circuit to the AD beam parameters; the analysis of thermal and mechanical cryostat modes.

A CRYOGENIC CURRENT COMPARATOR FOR THE LOW ENERGY ANTIPROTON FACILITIES AT CERN

M. Fernandes*, The University of Liverpool, U.K. & CERN, Geneva, Switzerland
J. Tan, CERN, Geneva, Switzerland,
C.P. Welsch, Cockcroft Institute & The University of Liverpool, Liverpool, U.K.

Abstract

Several laboratories have shown the potential of using Superconducting QUantum Interference Device (SQUID) magnetometers together with superconductor magnetic shields to measure beam current intensities in the sub-micro-Ampere regime. CERN, in collaboration with GSI, Jena university and Helmholtz Institute Jena, is currently working on developing an improved version of such a current monitor for the Antiproton Decelerator (AD) and Extra Low ENergy Antiproton (ELENA) rings at CERN, aiming for better current resolution and overall system availability. This contribution will present the current design, including theoretical estimation of the current resolution; stability limits of SQUID systems and adaptation of the coupling circuit to the AD beam parameters; the analysis of thermal and mechanical cryostat modes.

LOW-INTENSITY BEAMS CURRENT MEASUREMENT

Low-intensity charged particle beams present a considerable challenge for existing beam current diagnostics [1], this is particularly significant for coasting beams with average current below $1 \, \mu A$ which is the minimum resolution of DC Current Transformers. Other monitors, such as AC Current Transformers or Schottky monitors are able to measure low-intensity beam currents, but neither can simultaneously provide an absolute measurement, with a high current and time resolution, which is at the same time independent of the beam profile, trajectory and energy.

At CERN's low-energy antiproton decelerators, the AD and the ELENA (currently under construction) rings, circulate both bunched and coasting beams of antiprotons with average currents ranging from $300 \, nA$ to $12 \, \mu A$ [2]. Having a current measurement with the above mentioned characteristics would benefit the machine operation and optimization.

To meet these requirements, a low-temperature SQUID-based Cryogenic Current Comparator (CCC) is currently under development. Similar devices have already been developed for electrical metrology [3], and later for beam current measurements in particle accelerator [4]. The current, a collaboration between CERN, GSI, Jena University and Helmholtz Institute Jena aims to make this a fully operational device, with a prototype foreseen to be tested in the AD machine at CERN in 2015.

The main design specifications for the monitor are: beam current resolution $< 10 \, nA$; and measurement bandwidth $> 1 \, kHz$.

Overview of the functioning principle of the CCC

The CCC (see Fig. 1) works by measuring the magnetic field induced by the particle beam current. This field is concentrated in a high-permeability ferromagnetic pickup core, from which it is coupled into a Superconducting QUantum Interference Device (SQUID). These are highly sensitive magnetic flux sensors that permit sensing the weak fields created by the beam. A superconducting magnetic shield structure around the pickup-core, as described in [4, 5], renders the coupled magnetic field nearly independent of the beam position and makes the system practically immune to external magnetic field perturbations.
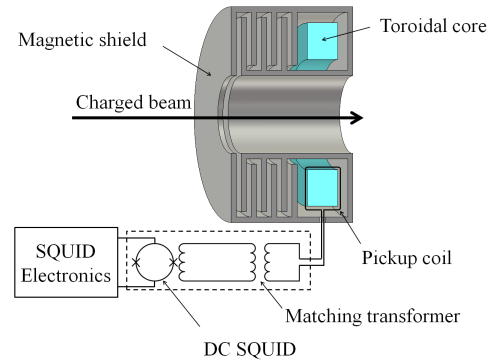

Figure 1: Schematic of the CCC.

CCC MONITOR DIMENSIONING

The AD CCC will in a first phase use a superconducting shield and pickup core developed by Jena University and Helmholtz Institute Jena. This core has a single turn inductance $L_P = 104 \, \mu H$, while the SQUID device [1] has the following parameters, input coil self-inductance $L_i = 1 \, \mu H$ and mutual inductance $M_i = 3.3 \, \phi_0/\mu A$ [2].

Coupling circuit and resolution

The circuit such as the one depicted in Fig. 2 will be used to couple the beam current signal into the SQUID. The transfer function of this circuit, defined as the change

[1]Manufactured by Magnicon GmbH.

[2]$\phi_0 = 2.0678 \times 10^{-15}$ Wb is the magnetic flux quantum which is the unit commonly used for magnetic flux when dealing with SQUID systems.

in the flux coupled to the SQUID per unit change in beam current $S_{I_B} = \Phi_S(t)/I_B(t)$, excluding the RC-shunt, is given by:

$$S_{I_B} = \left[\frac{M_i M_P M_f}{(L_P + L_1)(L_2 + L_i) - M_f^2} \right], \qquad (1)$$

where M_P is the mutual inductance between the beam current and the pickup core coil self-inductance L_P, M_f is the mutual inductance of the matching transformer and $L_{1,2}$ are the respective primary and secondary self-inductances (see Fig. 2).

Since the pickup core is made of a high-permeability material one can assume that $M_P \approx L_P$, provided that L_P is a single-turn coil. To optimally couple the signal to the SQUID, a matching transformer is used to adapt the high inductance of the pickup core with the much smaller inductance at the SQUID input. Optimizing S_{I_B} for the known values of L_P and L_i, and assuming a coupling factor of $k = 0.9$ one obtains:

- $L_1 = 239\,\mu H$

- $L_2 = 2.29\,\mu H$

- $S_{I_B} = 10.5\,\phi_0/\mu A$

Using a high inductance pickup core is desirable since it maximizes the signal coupling, but not if this increase in the inductance is obtained by increasing the number of turns in the secondary coil of the pickup-core, since then this would be acting as a current transformer with current transformation ratio $1/N_P$. The only options left are to increase the size of the core or the magnetic permeability of the ferromagnetic material.
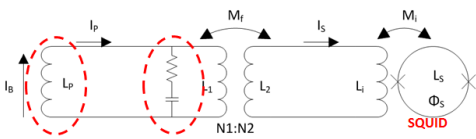

Figure 2: Circuit coupling beam current into SQUID magnetic flux density. In red are the elements with a low-pass effect.

Nanocrystaline soft magnetic materials are good candidates since these have very high real permeability and exhibit low losses particularly at low-frequencies. Additionally, different studies [6] have shown that these materials keep most of their magnetic properties when cooled down to $4.2\,K$. The material of the pickup core to be used in the first phase AD installation is Nanoperm [3]. Fig. 3 shows the complex permeability measurements performed by [7].

The permeability curves can be fitted to good agreement, with a first-order relaxation Debye model, provided that a

_____
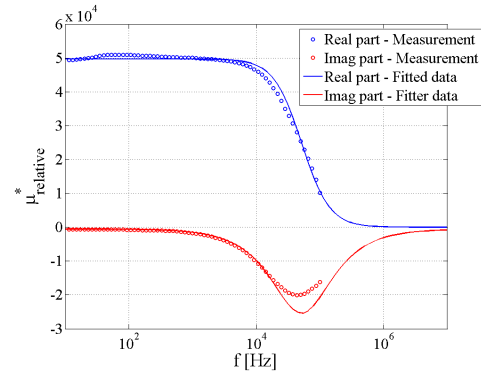[3] Produced by Magnetec GmbH.

Figure 3: Complex relative permeability of Nanoperm ferromagnetic cores. Measurements [7] and curve fitting.

constant imaginary term is added in order to account for the $1/f$ spectral noise behaviour at low frequencies [8].

$$\mu_r^*(f) = 1 + \frac{K_{spin}}{1 + i\frac{f}{f_{spin}^{res}}} - iK_{1/f} \qquad (2)$$

The obtained values for this model parameters are $K_{spin} = 49700$ for the DC magnetic susceptability, $K_{1/f} = 556$ for the DC imaginary magnetic permeability, and $f_{spin}^{res} = 51.5\,kHz$ for the resonant frquency of the spin magnetic moment.

The current resolution of the monitor will be fundamentally limited by the different noise contributions. The intrinsic noise level of the SQUID plus its read-out electronics for modern low-noise devices is of the order of $1.2\,\Phi_0/\sqrt{Hz}$, with corner frequency at $\leq 1\,Hz$. Using the fitted complex permeability functions, shown in Fig. 3, it is possible to calculate the induced noise from the ferromagnetic material via the fluctuation-dissipation theorem [9, 10]. This results in Eq. 3, where L_0 is the value of an equivalent air-inductor, L_i is the load inductance connected to the ferromagnetic core coil, T is the temperature and k_B is the Boltzman constant.

$$< I_C^2 >_{PSD} = \frac{4k_BT}{\omega L_0} \left(\frac{\mu''(\omega)}{[L_i/L_0 + \mu'(\omega)]^2 + \mu''(\omega)^2} \right) \qquad (3)$$

The calculated noise spectral density from the pickup core, as well as the SQUID and read-out electronics is shown in fig 4. These are calculated as flux coupled to the SQUID.

External noise sources may also adversely impact the measurement resolution. Particularly in an accelerator environment, where many possible sources of mechanical vibrations, stray magnetic fields, and RF interference are present. The magnitude of these noise components can only be accurately known from measurements at the installation location. Nevertheless one can estimate the impact on the current resolution by assuming different values for an additional constant spectral noise component that accounts for all the external perturbations.

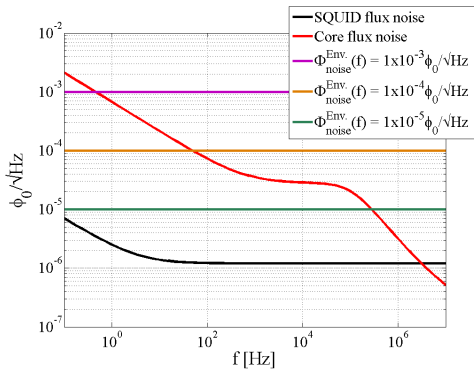Combining the different noise components and parameterising the environmental noise contribution, the achiev-

Figure 4: Spectral density of the expected magnetic flux noise coupled to the SQUID.

able beam current resolution (considering a bandwidth of $1\,\text{kHz}$) can be estimated. The results are shown in Fig. 5. Assuming that $\Phi_{\text{noise}}^{\text{env.}} = 1 \times 0^{-3}\phi$ (purple curve) the ex-
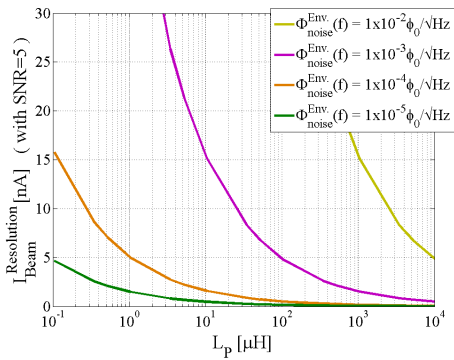

Figure 5: Expected noise-limited beam current resolution as a function of the pickup inductance, taking into account the known SQUID and core components, and assuming different values for the combined unknown average environmental sources.

pected current resolution for $L_P = 100\,\mu\text{H}$, with $SNR = 5$, is $5\,\text{nA}$, which complies with the specification.

Values for the first CCC monitor installation at GSI, reported in [4], using an older SQUID technology, and with a less performant magnetic core and shield, indicate noise density values of $2\ldots23 \times 10^{-4}\,\phi_0/\sqrt{\text{Hz}}$. Recent measurements, performed at GSI with a CCC installed in a beam line, and equipped with a modern SQUID system, indicate much smaller noise figures, with perturbation peaks of the order of $10^{-5}\,\phi_0/\sqrt{\text{Hz}}$ and noise floor $10^{-6}\ldots10^{-5}\,\phi_0/\sqrt{\text{Hz}}$, over a frequency range from $10\,\text{Hz}$ to $10\,\text{kHz}$. This indicates that considering an average environment noise of $\Phi_{\text{noise}}^{\text{env.}} = 10^{-4}\,\phi_0/\sqrt{\text{Hz}}$ (orange curve in the plots) is a good conservative estimation.

Flux-Locked-Loop (FLL) and slew-rate limitations

SQUID devices are unparalleled in the sensitivity they exhibit to magnetic flux variations. The model chosen for the AD monitor has a maximum value of $2579\,\mu\text{V}/\phi_0$. However, this only holds in small regions of the periodic $V(\Phi)$ transfer function. To linearise this response and increase its dynamic range most common readout schemes implement a flux feedback loop - a so called Flux-Locked Mode (FLL) - as shown in Fig. 6. This keeps the SQUID
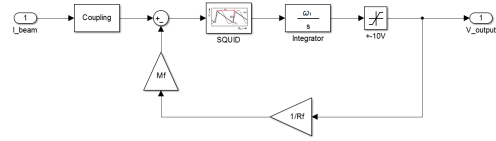

Figure 6: SQUID readout Flux-Locked Mode.

operating at a constant working point ($\Phi_{\text{SQUID}} = \text{constant}$), while the measurement output is given by the output voltage of the integrator. The bandwidth of the system in FLL readout mode is given by

$$f_{BW} = \frac{V_\Phi M_f}{R_f} f_I, \tag{4}$$

where, M_f is the mutual inductance of the SQUID feedback coil, R_f is the feedback resistance converting output voltage into feedback current, and f_I is the gain of the preamplifier and integrator.

In order for the SQUID to be able to track input signals with a high slew-rate, while keeping a constant working point and avoiding the occurrence of flux jumps, the closed loop bandwidth (given by Eq. 4 and typically limited to a few MHz) needs to be high enough for the feedback loop to react in a short time, driving the error signal ($\Phi_e = \Phi_{signal} - \Phi_{feedback}$) close to 0. However, if the bandwidth is too high, this will increase the amplitude of the amplified noise that is fed-back into the SQUID, increasing the probability of fast changing flux signals that cannot be compensated by the feedback loop, thus imposing a limit on the maximum bandwidth that can be set for the FLL loop. The condition for stable operation can be conservatively defined to be

$$|\delta\Phi_e| < \phi_0/2. \tag{5}$$

Assuming a Gaussian distribution for the total noise, it is possible to calculate the maximum allowed slew rate as a function of the FLL bandwidth [11]. This is shown for different average spectral noise density values in Fig. 7. In this calculation the maximum allowed flux-jump rate was assumed to be 1 per hour. This is considered reasonable as a calibration of the CCC can be performed before the start of each AD cycle, which has the duration of $85\,\text{s}$.

If one considers an average $\Phi_{noise} = 10^{-5}\,\phi_0/\sqrt{\text{Hz}}$, the stability region for the system will be roughly bounded by:
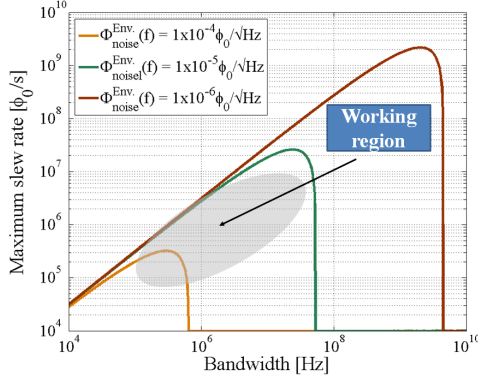
Figure 7: Maximum slew-rate for different RMS SQUID flux noise levels as a function of the FLL loop bandwidth, for a flux jump rate $< 1/\text{hour}$.

- Slew rate limit for input signal: $d\phi/dt < 5\,\text{M}\phi_0/\text{s}$

- FLL loop bandwidth limit: $f_{3dB} < 20\,\text{MHz}$

During AD beam injection, when the average current jumps from 0 to $12\,\mu\text{A}$, the slew-rate is $400\,\text{M}\phi_0/\text{s}$. This can be reduced by decreasing the flux coupling or by low-pass filtering before the SQUID input. The latter is preferable since it does not entail a loss of current resolution. Given this, the design includes an RC-shunt in the coupling circuit, with [4] $R = 1\,\Omega$ and $C = 10\,\mu\text{F}$, which has the effect of attenuating the input with a second-order filter as shown in Fig. 8.
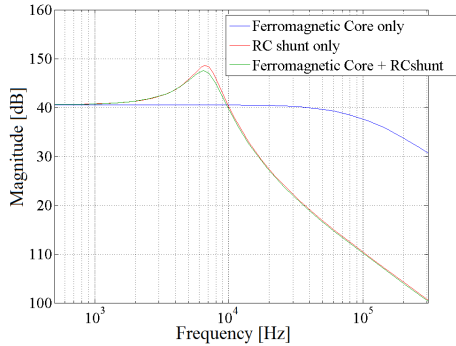

Figure 8: Coupling circuit transfer function with low-pass filtering effect from frequency dependent permeability, RC-shunt, and both combined.

When the injected AD beam couples to the SQUID through this coupling circuit, the maximum slew-rate is reduced to $3\,\text{M}\phi_0/\text{s}$. The resonant peak will cause an overshoot on the signal to be measured but the settling time (to within 1%) is calculated to be $0.45\,\text{ms}$, considered acceptable compared to the overall measurement bandwidth requested for the monitor.

It should also be mentioned that the delays t_d introduced by the different components in the FLL loop, which are normally dominated by the cables connecting the SQUID device to the room-temperature electronics, may be another source of instability depending on the cable length. Keeping $f_I t_d < 0.08$, as explained in [12], results in the maximal flat frequency response and guarantees that the phase margin at the cut-off frequency does not come close to possibly unstable values. For a $1\,\text{m}$ cable the typical delay is of the order of $\sim 10\,\text{ns}$ resulting in a maximum achievable value of $f_I = 20\,\text{MHz}$ [5] for systems with electronics at room-temperature.

CRYOSTAT DESIGN

A new cryostat is being developed at CERN to house the CCC monitor and allow for its integration in the AD-ring. The main requirements for this cryostat are:

- Long term operation at $4.2\,\text{K}$

- Annular cryostat with the inner wall of the vacuum vessel acting as the beam pipe

- Ceramic insulating rings to break the beam image current and allow magnetic coupling to the outside

- A supporting structure optimised for stiffness and mechanical resonances to minimise perturbation of the CCC

- Accessibility of the CCC without the need to break the beam vacuum

The CCC will be cooled by a liquid Helium (LHe) bath supplied by an external re-condensation unit based on a pulse tube cryocooler. The evaporated He will be circulated through the radiation shield to cool it down to an intermediate temperature of $50 - 70\,\text{K}$, after which it will return into the re-condensation unit for liquefaction. This will enable stand-alone operation, with no need for periodic refills with LHe. Modern, commercially available, pulse tube cryocoolers can provide up to $1\,\text{W}$ of cooling power at $4.2\,\text{K}$. Integrated re-condensing units, are slightly less efficient, providing cooling powers ranging from $> 0.3\,\text{W}$ to $> 0.8\,\text{W}$ [6]. Fig. 9 shows a longitudinal cut through the different vessels of the cryostat. The two most challenging aspects of the design are:

- The proximity of components between the CCC (ID $185\,\text{mm}$) and the beam pipe (OD $103\,\text{mm}$), where, two sets of ceramic isolator rings and associated bellows are required to prevent the flow of beam image currents.

- The design of the LHe vessel support structure which should be both stiff and have low thermal conductivity.

---

[4]The largest capacitance available for small-sized capacitors at cryogenic temperatures is $\leq 1\,\mu\text{F}$.

[5]With increased t_d the FLL bandwidth is in fact slightly increased with $f_{3dB} = 2.25 f_{I,\text{max}}$ [12].

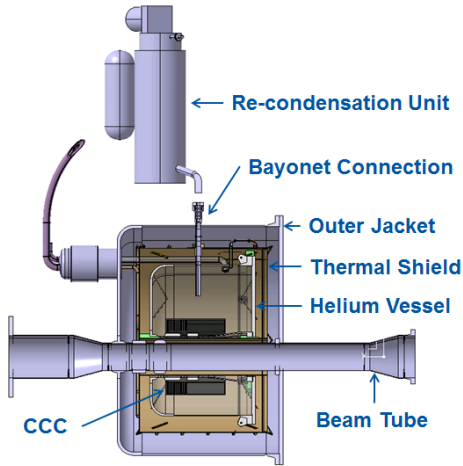[6]Example of single cryocooler units developed by Cryomech.

Figure 9: Cryostat longitudinal view

It has been decided to use Kevlar 49 cables rather stainless steel bars to support to LHe vessel due to Kevlar's superior heat conductivity to stiffness relationship. The known sources of mechanical perturbations originate in the cryocooler ($f < 2\,\mathrm{Hz}$) and the He compressor connected to the re-condensation unit ($f = 50\,\mathrm{Hz}$). The design of the support structure therefore tries to increase its first resonant frequency above the $50\,\mathrm{Hz}$. This can be achieved by increasing the number of support cables and their diameter. However this will also increase the heat in-leak. In order to optimize the support structure, an analysis combining the structural mode frequencies and the heat load was performed as a function of the number supporting Kevlar cords and their diameter. The results are shown in Fig. 10. A
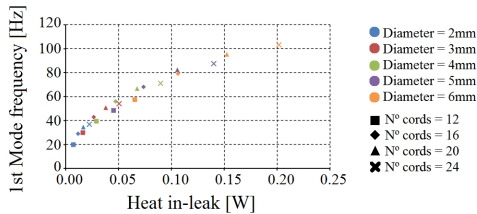

Figure 10: Frequency of the first mechanical mode versus the heat load into the 4.2 K vessel for different number of Kevlar support cables and cable diameter.

support structure with a total of 16 support cables, of $4\,\mathrm{mm}$ diameter was found to be a good compromise, resulting in a first mode frequency close to $60\,\mathrm{Hz}$ while maintaining a small heat load.

The total estimated heat load, shown in table 1, in the $4.2\,\mathrm{K}$ surface equals $0.422\,\mathrm{W}$, corresponging to an Helium evaporation rate of $14\,\mathrm{l/day}$. Modern recondensing units with a single pulse tube cryocooler can generate from $> 10\,\mathrm{l/day}$ to $> 27\,\mathrm{l/day}$, depending on model and working conditions.

Table 1: Estimated heat load for radiation shield surface (at 50 K) and LHe vessel surface (at 4.22 K).

	50 K [W]	4.2 K [W]
Kevlar supports (16×)	0.5864	0.0473
Bayonet + Safety Valve	3.6065	0.1832
Cryostat instrumentation	0.8185	0.0527
Heater wires	0.0195	0.0004
SQUID cabling	0.0162	0.1798
Total	**5.0471**	**0.4219**

CONCLUSIONS

The design and dimensioning of the main parts of a prototype CCC monitor for the AD machine at CERN has been presented. The expected performance based on theoretical analysis, as well as analysis of stability conditions required for its reliable operation, were evaluated. The conclusion is that considering all the particularities of this monitor it should be possible to construct a system for the AD-ring that meets the requirements. In addition a stand-alone cryogenic system has been designed that should allow maintenance free-operation during AD running.

This theoretical analysis of the CCC performance will provide a good basis for the benchmarking of this monitor once it is installed for beam tests in 2015.

ACKNOWLEDGMENT

REFERENCES

[1] D. Belohrad, "Beam Charge Measurements," WEOC01, DIPAC2011 proceedings.

[2] M.F. Fernandes, "Cryogenic Current Comparator as Low Intensity Beam Current Monitor in the CERN Antiproton Decelerators," MOPF25, IBIC2013 proceedings.

[3] I.K. Harvey, Rev. Sci. Instrum. 43 (1972) 1626.

[4] A. Peters et al., "A cryogenic current comparator for the absolute measurement of nA beams," BIW98, Standford, May 1998, (p. 163), AIP conference proceedings.

[5] K. Grohmann et al., Cryogenics 16(10) (1976) 601.

[6] A. Steppke et al., "Application of LTS-SQUIDs in Nuclear Measurement Techniques," IEEE Transactions on Applied Superconductivity 19(3), p. 768 (2009).

[7] R. Geithner et al., Cryogenics 54 (2013) 16.

[8] G. Durin et al., "Low temperature properties of soft magnetic materials: Magnetic viscosity and 1/f thermal noise," Journal of Applied Physics 73(10), p. 5363 (1993).

[9] S. Vitale et al., "Thermal magnetic noise in rf SQUIDS coupled to ferromagnetic cores,". Journal of Applied Physic 65(5), p. 2130 (1989).

[10] N. R. Hutzler et al., "Low temperature, high frequency permeability of Metglas 2714A and its potential for use as a core material for EMI filters," Cryogenics 47(5-6), p. 279 (2007).

[11] R. H. Koch, "Maximum theoretical bandwidth and slewrate of a dc SQUID feedback system," IEEE Transactions on Applied Superconductivity 7(2), p. 3259 (1997).

[12] D. Drung and M. Muck, "Chapeter 4: SQUID Electronics", In: J. Clarke and A. Braginski, *The SQUID Handbook. Vol. I: Fundamentals and Technology of SQUIDS and SQUID Systems. Materials and Manufacturing Processes, (Weinheim: Wiley-VCH, 2005).*